Hydrokinetic propeller turbines. How many blades?

Antonio C. P. Brasil Junior, Rafael C. F. Mendes, Julian Lacroix, Ricardo Noguera, Taygoara F. Oliveira

Hydrokinetic propeller turbines. How many blades?

[1*] Brasil Junior, Antonio C. P.; [1]Mendes, Rafael C. F.; [2]Lacroix, Julian; [2]Noguera, Ricardo; [1]Oliveira, Taygoara F.

ABSTRACT

A design study of propeller hydrokinetic turbines is presented. The main objective is to evaluate the optimized geometry for horizontal axis hydrokinetic turbines, take into account the runner design with a different number of blades. The optimized blade geometry is determined by the Glauert theory for axial free flow turbines (hydrokinetic and wind turbines). The performance of the different blades is evaluated in the entire range of operating conditions, using Blade Element Momentum Theory (BEMT). Computational Fluid Dynamics (CFD) computations were also carried out to evaluate the detailed features of the fluid flow.

KEYWORDS: Hydrokinetic turbines. Propeller horizontal axis turbines. BEM methods. Glauert theory.

1. INTRODUCTION

The hydrokinetic turbines are placed in a context of an emergent renewable technology that had an important and fast innovation development during the last decade. Low environmental impact conversion systems can be implemented using this technology for sites with hydrokinetic potential in rivers or in marine environment [1-5]. The kinetic energy of the water streams can be converted to electricity by means of different models of free flow hydro turbines and the modern design methodologies have been employed to obtain optimized machines, augmenting the performance of the turbines and reducing the cost of the technology. It is an important alternative for the sustainability of small and medium energy systems, with applicability in many worldwide regions.

One considers, in the present paper, a horizontal axis propeller turbine with a diameter D, with N_b blades, with a rotation speed of ω (see Figure 1). Those machines are aligned to the stream direction, converting the kinetic energy of the water flow, with velocity V_0, to mechanical power. The turbines can be installed in the bottom of a river or in a marine site (Figure 2). The machines can be placed also near the free surface using floaters or pylons. From the turbomachinery technology point of view, those turbines belong to the same family of wind turbines or to the propeller hydraulic machines. The design approaches employed for those conventional turbines can be adapted for this specifically situation [6-9].

The main problem to be discussed here is the influence of the number of the blades for given operating conditions and the desired performance level. To answer this question, few hydrodynamical design approaches can be employed. The first possibility is to use the design approach to optimize runner geometries of conventional axial hydraulic turbines (Kaplan or propeller). Another possibility is to employ the design approach of wind turbines. Both methodologies, used to define the best shape of the blades, are very close one to each other, but some differences have to be pointed out.

The first approach inherits the aspects for the classical dimensioning of the axial runners in conventional hydraulic machines. It is based on the integral equations of fluid mechanics (Euler equation) and in the determination of the hydrodynamical efforts using the velocity triangles on the runner inflow and outflow cross sections. This methodology has been historically employed to the "confined" runners and many classical developments have evolved to obtain geometries with high hydraulic efficiency (see Rodrigues et al. [10], Cruz et al. [11] for instance). The main problem with this approach is that it does not take into account the condition of the free flow and the reduction of the axial velocity in the front of the runner. To be precise, an optimum runner designed to a confined flow rate (close to that one related to the velocity V_0) can have the worst performance in free flow condition. It is justified by the fact that the flow blockage effect, dependent on the geometry of the runner and its rotation speed, reduces the flow velocity in the inflow plane in front of the blades. Consequently, it decreases substantially the converted hydrodynamics power, which is scaled to the cube of the effective inflow velocity.

Considering the arguments of the last paragraph, the wind turbines methodologies [12-14], which considers as its hypothesis the free flow condition and its variation through the axial direction, seems more adapted to the design of free flow runners. Taken it into account, the methodology for the design of free flow turbines (wind and hydrokinetic) will be employed in the present study.

In general, the free flow runners design approach is based on the Glauert theory [15], with several improvements for applications in wind turbines [15-18], propellers [19] and hydrokinetic devices [9]. Some *ad hoc* corrections associated with complex physical flow features (wake hydrodynamics, tip blade effects, etc.) have been proposed and the cavitation limits for the water flow have been also considered, constraining the rotation speed of the runner in particular for large hydrokinetic machines [14].

The key point of the Glauert formulation lies in the actuator disc approach and the Boundary Element Momentum Theory (BEMT), which considers the balance of linear and angular momentum in the runner, as well as an estimate of the hydrodynamic forces in each section of the blade. In the present paper, this methodology will be employed for the blade shape design and to the performance analysis, evaluating the influence of the number of blades for optimized geometries to runners with 2 to 4 blades in the performance of the turbine. The BEMT methodology is validated by comparisons of the performance estimates to the CFD computations.

[1]Universidade de Brasilia. Faculdade de Tecnologia. Laboratório de Energia e Ambiente. 70910-900 Brasília. DF. BRAZIL. *Corresponding Author – Email: brasiljr@unb.br
[2]Ecole Nationale d'Arts et Métiers. Laboratoire DynFluid, Paris-France.

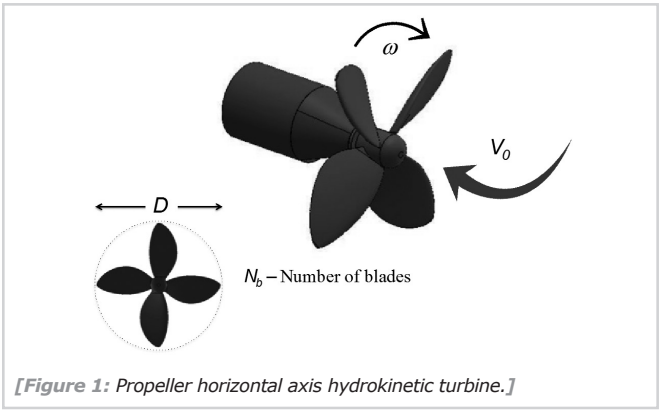

[Figure 1: Propeller horizontal axis hydrokinetic turbine.]

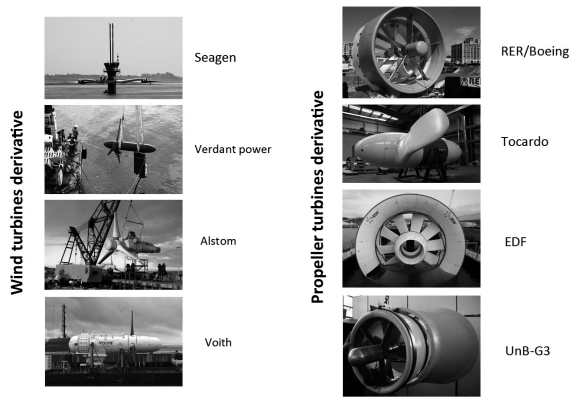

[Figure 2: Example of commercial and experimental models of horizontal axis hydrokinetic turbines [22-29].]

2. MATERIAL AND METHODS

2.1 Rotor kinematics

The performance of a hydrokinetic turbine is expressed by the power coefficient, which is parameterized by its dependence to the Tip Speed Ratio, denoted respectively by C_p and λ. Those variables are classically defined as

$$C_P \equiv \frac{P}{1/2 \rho A V_0^3}, \tag{1}$$

$$\lambda \equiv \frac{\omega R}{V_0}. \tag{2}$$

In Equations (1) and (2) *P*, *A* and *R* denote respectively the power, area and radius of the rotor, and ρ is the water density.

In other to define the flow kinematics of the machine in the runner, firstly a parameterization of the axial velocity on the rotor inflow plane is written as (see Figure 3):

$$V = (1-a)V_0. \tag{3}$$

Additionally, on the outflow plane, the tangential velocity in the rotating wake – in opposite to the rotor rotation, can be expressed by a model of free vortex written as

$$V_\theta = 2\omega r a'. \tag{4}$$

Equations (3) and (4) introduce the axial and tangential induction factors denoted by a and a', respectively. Those variables are dependent to the radial position r.

In the rotor middle-plane (between A and B sections in Figure 3) and at a radial position r, the velocity triangle can be defined as illustrated in Figure 4, such that the inflow angle ϕ, can be determined by

$$tan\phi = \frac{(1-a)V_0}{(1+a')\omega r} = \frac{(1-a)}{(1+a')\lambda_r}, \tag{5}$$

$$\text{with } \lambda_r \equiv \frac{\omega r}{V_0}.$$

Considering the similarity of the two triangles illustrated in Figure (4b), an additional relation yields:

$$tan\phi = \frac{a'\omega r}{V_0 a} = \frac{a'}{a}\lambda_r \tag{6}$$

From Equations (5) and (6) a kinematic relationship between a and a' can be obtained in the form

$$a'(1+a')\lambda_r^2 = a(1-a). \tag{7}$$

Using this equation, for a specific value of axial induction factor a and for a local velocity ratio λ_r, the tangential induction factor can be calculated from the Equation (7) by

$$a' = \frac{1}{2}\left(\sqrt{1+4\lambda_r^{-2}a(1-a)} - 1\right). \tag{8}$$

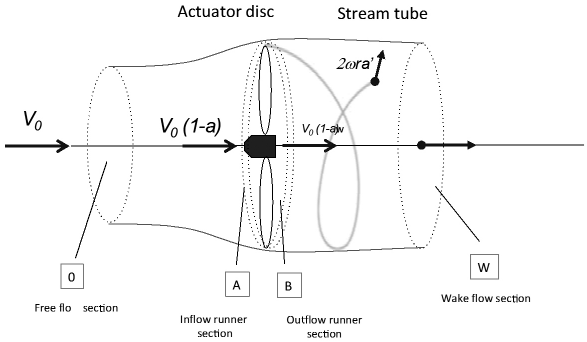

[Figure 3: Flow through an axial runner.]

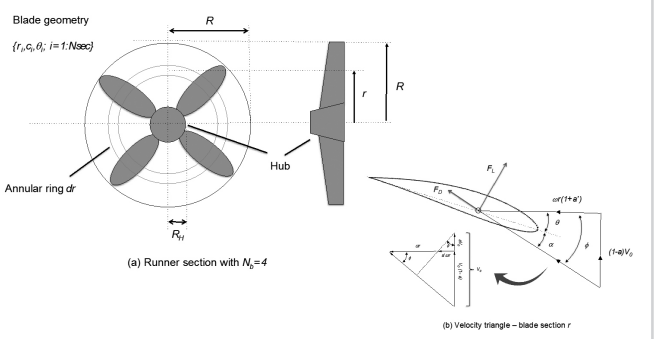

[Figure 4: Machine kinematics – Velocity triangles in a blade section at r and radial cross-section dr.]

2.2 Axial and angular momentum balance

The axial and angular momentum conservation principles, applied to the fluid flow through the runner (from sections A to B), give us expressions for the thrust and torque differentials as resulting from an integral 1D balance in an anular section of radius dr (for more details see [12] or [13] for instance) as being

$$dT = 4\pi r \rho V_0^2 a(1-a)dr, \quad (9)$$

and

$$dM = 4\pi r^3 \rho V_0 \omega (1-a)a'dr. \quad (10)$$

In those equations, *dT* and *dM* denote the parcel of the thrust and torque in the runner related to the section.

The hydrodynamic power in dr can be computed from Equation (10) as

$$dP = \omega dM = 4\pi r^3 \rho V_0 \omega^2 (1-a)a'dr, \quad (11)$$

Or, in a dimensionless form,

$$dC_P = \frac{8}{\lambda}(1-a)a'\lambda_r^3 \, d\lambda_r \quad (12)$$

Therefore, the power coefficient for entire runner can be computed by integrating Equation (12) in the radius range given

$$C_P = \frac{8}{\lambda}\int_0^{\lambda}(1-a)a'\lambda_r^3 \, d\lambda_r \quad (1\ 3)$$

The observant reader should notice that λ_r could be interpreted as a dimensionless radius. Equations (12) and (13) establishes a direct dependence of the runner performance to the radial distribution of the pair *{a,a'}*. Some important remarks have to be pointed out:

Remark 1: The optimization of the performance lies in the maximization of the C_p, that is directed related to the maximum value of the term *f(a,a')=a'(1-a)*.

Remark 2: Classically, the Betz theorem establishes an optimum of C_p equal to 16/27, which is equivalent to *a=1/3* and *a'=0* (see [12] for instance). The equations (12) and (13) show that this limit is not valid in the case of a rotating wake, and a new optimum point has to be considered in this more realistic situation, taking into account the changing in the angular momentum in the fluid flow through the rotor.

Remark 3: Considering the relationship between *a'* and *a*, given by the Equation (8), the optimization problem related the search of the maximum condition for *f(a,a')* can be simplified to a one-dimensional problem, only dependent on the variable a, considering that *a'=a'(a)*. It is the aim of the Glauert theory [14].

2.3 Optimum flow conditions for runner design

Given the turbine nominal operation variables $\{\omega, V_0\}$, which defines the values of λ, and for each radial position λ_r. The best value of dC_p, related to the maximum condition of *f(a,a')*, is simply obtained by the derivative of the function *f* to a, i.e.:

$$\frac{df}{da} = (1-a)\frac{da'}{da} - a' = 0 \quad (14)$$

From Equations (7) and (8), substituting the term *da'/da* in Equation (14), the following conditions for *{a,a'}* verifies the maximum power coefficient increment in Equation (12), i.e.:

$$16a^3 - 24a^2 + 3(3-\lambda_r^2)a - (1-\lambda_r^2) = 0, \quad (15)$$

and

$$a' = \frac{1-3a}{4a-1} \quad (16)$$

Therefore, for a given value of λ_r, Equations (15) and (16) can be solved for the values of *{a,a'}*. After all, Equation (5) can be also employed to obtain the value of the inflow angle ϕ.

The mathematical problem to determine the optimum axial induction factor, given by the Equation (15), can be solved numerically using any non-linear solver (e.g. **fsolve** function in Matlab). Some analytical approaches can also be used to obtain the third order polynomials roots (see [21], for instance).

Considering the optimum conditions for the fluid flow through the rotor, the following algorithm can be employed to determine the first group of variables for the blade design:

Algorithm A.1: Optimum flow conditions

Step 1: Given the design data $\{\omega, V_0, D\}$

Step 2: Compute λ and $\{\lambda_{r,i}; i=1:Nsec\}$

Step 3: Solve non-linear problem (15) obtaining $\{a_i; i=1:Nsec\}$

Step 4: Compute $\{a'_i; i=1:Nsec\}$, using the Equation (16).

Step 5: Compute $\{\phi_i; i=1:Nsec\}$, using the Equation (5).

Step 6: Compute an estimate of the maximum C_p using the numerical integral (13).

In this algorithm the blade is divided in Nsec radial sections.

2.4 Blade Element Momentum Theory

The BEMT method is a useful methodology to blade design of free flow turbines. It can be also employed to compute the machine performance for any value of λ. This method is presented in many textbooks and some additional *ad hoc* corrections have been formulated and reported in the literature, allowing good realistic results for the turbine performance modeling [16-18].

In the BEMT, Equations (9) and (10) are complemented by the computation of the hydrodynamic forces in a blade element *dr* by the hydrofoil theory. For a rotor with N_b blades the thrust and the moment in a section of width *dr* can be computed by:

$$dT = \frac{1}{2}\rho N_b c \frac{V_0^2(1-a)^2}{F(r,N_b).sin^2\phi} C_n dr \quad (17)$$

and

$$dM = \frac{1}{2}\rho N_b c \frac{V_0(1-a)\omega r(1+a')}{F(r,N_b).sin\phi cos\phi} C_t r dr. \quad (18)$$

In Equations, (17) and (18) c is the chord length and F(r,Nb) is a correction function used to take into account complex flow phenomena in the rotating blades (e.g tip and hub losses). In the present work, Prandtl's tip and hub losses correction are considered, using:

$$F_{tip} = \frac{2}{\pi} cos^{-1}\left[exp\left(-\frac{N_b}{2}\frac{R-r}{r\,sin\phi}\right)\right], \quad (19)$$

$$F_{hub}\frac{2}{\pi} cos^{-1}\left[exp\left(-\frac{N_b}{2}\frac{r-R_h}{r\,sin\phi}\right)\right], \quad (20)$$

and

$$F(r,N_b) = F_{tip}.F_{hub}. \quad (21)$$

In Equations (17) and (18) the variables Cn and Ct are calculated using the lift and drag hydrofoil coefficients (CL and CD) as

$$C_n = C_L cos\phi + C_D sin\phi \quad (22)$$

and

$$C_t = C_L sin\phi - C_D cos\phi. \quad (23)$$

The NACA four digits foils are used in the present work, with parameters extracted from international databases for its geometry. The polar curves ($C_L(\alpha)$ and $CD(\alpha)$) are obtained from the open source code XFOIL [20].

From a design point of view, Algorithm A.1 give us the values of the induction factors (*a* and *a'*) and the inflow angle ϕ, which establishes the optimized flow conditions for each radial position. The rotor design is complemented with the definition of the blade shape, expressed by the chord c and twist angle θ for different sections distributed through its length, i.e., $\{c_i,\theta_i;\ i=1:Nsec\}$.

Using Equations (9) and (17), and estimating the tip and hub losses from (21), an optimal relation for the chord radial distribution can be explicitly obtained in the form

$$\frac{c(r)}{R} = \frac{8\pi}{N_b}\frac{a}{(1-a)}F(r,N_b)\frac{sin^2\phi}{C_n}\frac{r}{R} \qquad (24)$$

The blade-twist angle is obtained by taken into account an optimum attack angle of the foil. In the present paper, the optimum attack angle α_{op} is defined as the angle related to the maximum value of C_L/C_D. Therefore, for a given hydrofoil characteristics, with optimum attack angle of α_{op}, the pitch angle can be computed from the inflow angle (Equation (5)) using

$$\theta = \phi - \alpha_{op}. \qquad (25)$$

For rotors with a number of blades greater than four and high solidity ($\sigma \equiv N_b c/(2\pi r)$, the hydrodynamic interference of the flow through the neighbor's blades has to be considered. A correction interference factor related the cascade flow, which is dependent on the solidity and the twist angle, can be taken into account, changing the Equation (22) to

$$C_n = F_{casc}C_L cos\phi + C_D sin\phi. \qquad (26)$$

The classical correction factor F_{casc} proposed by Weinig [30] was updated in the present work to consider the variation of chord lengths along the radial position, providing a corrected version of C_n.The original plot proposed by Weinig, showed in Figure 5, was digitalized and a spline fitting is applied to obtain a Matlab function $F_{casc}(\sigma^{-1},\theta)$. This correction is currently assumed for the situations with $\sigma^{-1}<3$.

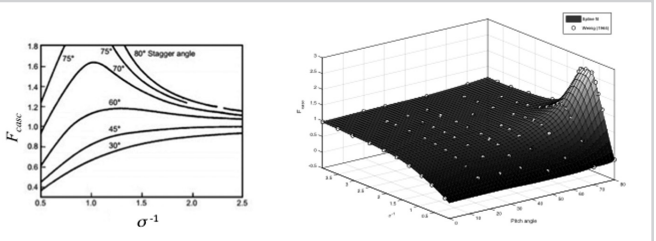

[Figure 5: Cascade flow correction [30] – Original plot and fitted surface.]

The mathematical formulation present on the last sections allows the proposition of the following algorithm to obtain the blade geometry:

Algorithm A.2: Blade geometry

Step 1: Given the design data Nb and variables obtained in the algorithm A.1 $\{a_i\phi_i;\ i=1:Nsec\}$

Step 2: Run XFOIL to obtain hydrofoil polars and $\{\alpha_{op}, C_L(\alpha_{op}),C_D(\alpha_{op})\}$

Step 3: Compute the twist angle $\{\theta_i=\phi_i-\alpha_{op};\ i=1:Nsec\}$

Step 4: Compute chord $\{c_i;\ i=1:Nsec\}$, using the Equations (21), (22) and (24).

Step 4: Compute σ^{-1} and correct the values of chord dimension if it is necessary.

2.5 Influence of the number of blades in runner design

The optimized blade geometry, issued from the methodological approach presented in the last sections, is explicitly related to the number of blades by means of the Equation 24. It is clear that for a greater number of blades thinner shapes are obtained (smaller chord dimensions).

For a design condition of a given tip speed ratio λ, the optimum inflow conditions $\{a.a',\phi\}$ give only one optimum design value of C_p (from algorithm A.1 and Equation 13). It is independent of the number of blades. On the other hand, the shape of the blade, given by the Equation (22) for the chord length, is dependent on the number of blades.

The volume of the entire rotor is related to the amount of material involved in the manufacturing the rotor. From the Equation (22), the dimensionless blade volume can be calculated by the following relation:

$$C_n = F_{casc}C_L cos\phi + C_D sin\phi. \qquad (26)$$

In this equation, Af is the dimensionless area of the standard airfoil section.

The volume depends on to the number of blades through the term $[F(r,N_b)/N_b)]$, which is a decaying function of Nb. This is an indication that the amount of material necessary to rotors manufacturing is also a decaying function of the number of blades. This methodology preserves the estimation of the power coefficient in optimum conditions for any number of blades.

Some works on wind turbine design report that rotors with a larger number of blades have slightly better power coefficients values (Duquette et al. [31]). It is a key point that will be investigated in the next section, using numerical methodologies to evaluate the performance of the different runners configurations. It is not clear, just at this point, that it is verified in the framework of BEMT-Glauert mathematical formulation for blade optimum blade design.

3. RESULTS AND DISCUSSIONS

3.1 Optimized blade geometry

The design methodology, presented in section 2 and summarized in algorithms A.1 and A.2, was implemented in a Matlab code. It allows us to compute the blade shape for a given set of input parameters$\{N_b, U_o, \omega\}$. The blade radius - *R*, is defined considering the target machine power. An iterative approach can be used, computing successively the power coefficient (from Equation (13)) and the nominal Tip Speed Ratio, up to the convergence to the desired power.

In the present paper, the blade design methodology uses the foil NACA4415 geometry, with polars curves obtained from the software XFOIL with a typical Reynolds number of 1.0e+06. Only the value of α_{op} and the evaluation of $C_{L,op}$ and $C_{D,op}$, are needed for the algorithm A.2.

Figure (6) presents the twist angle for a four blades rotor, for different values of λ. The associated C_p (which is independent of the number of blades) is obtained for whole range of tip speed ratio. It is a classical result that can be used to define preliminarily some design parameters (rotation speed for instance).

In Figure (7), different blade geometries are presented for rotors with four blades. This result shows that the thinner shapes are obtained for faster machines. Unfortunately, the tip cavitation is a constrain that limit the machine rotation speed and consequently the design tip speed ratio. It can be circumvented by means of an alternative chord design that

consider the cavitation limit [4], which in a practical point of view augments the dimension of the chord near to the tip.

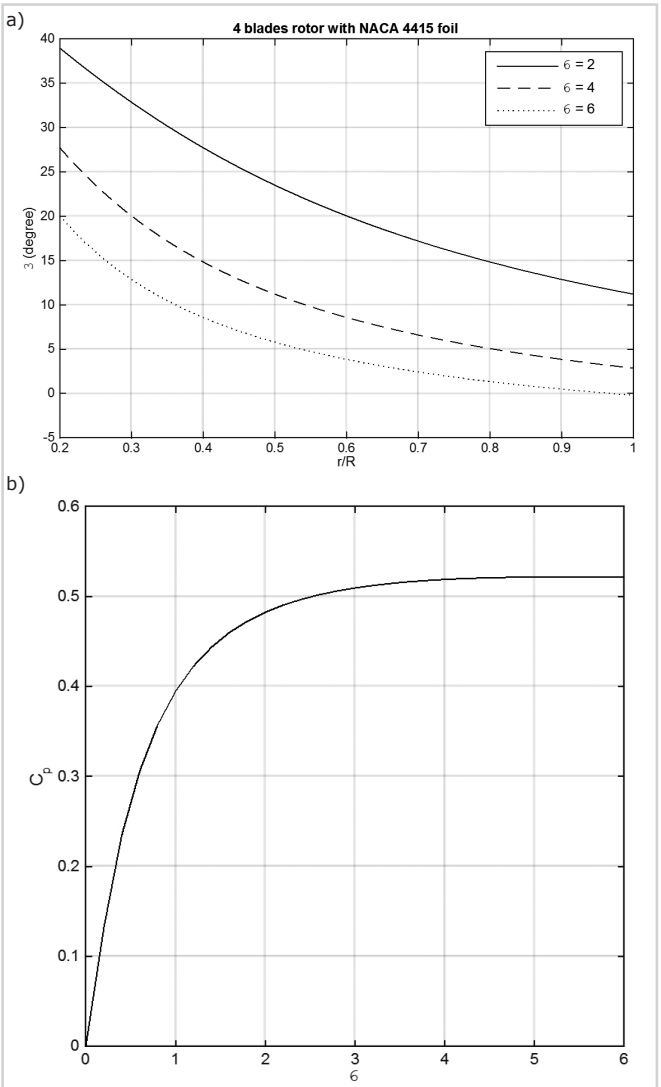

*[**Figure 6:** (a) Blade twist and (b) power coefficient for optimized conditions w/hub and tip corrections.]*

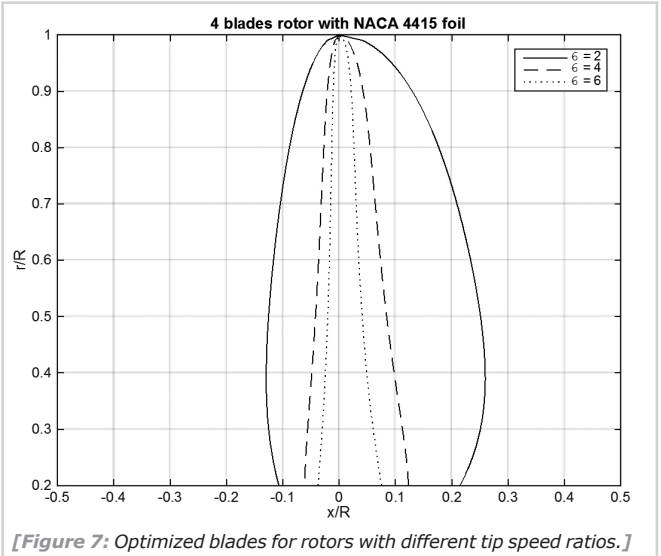

*[**Figure 7:** Optimized blades for rotors with different tip speed ratios.]*

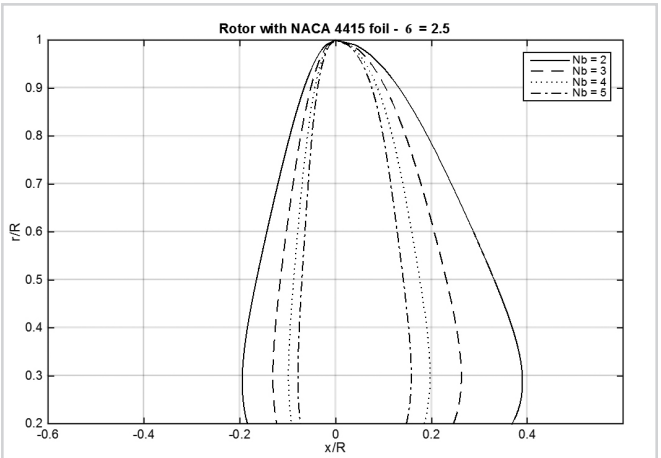

*[**Figure 8:** Optimized blades for rotors with different tip speed ratios.]*

On Figure (8), blade geometries for rotors with a different number of blades are illustrated. The 3D view is also shown in Figure (9). Rotors with many blades are related to the thinner shapes. The estimated power coefficients for all rotors are the same (considering the present the design methodology). The volume of the blades is smaller for rotors with a greater number of blades as shown in Figure (10). It is also observed in Equation (24).

All of those prelimina results are direct consequence of the design algorithm, with all classical ad hoc corrections (Tip, Hub, and Cascade). A better performance estimate will be computed in the next section

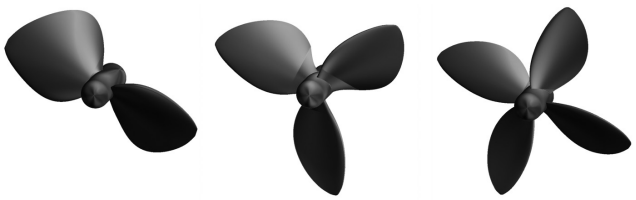

*[**Figure 9:** Rotors with different number of blades.]*

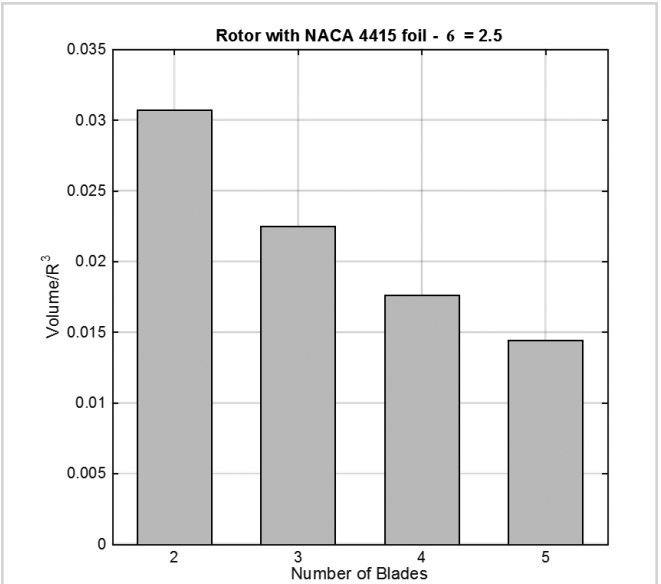

*[**Figure 10:** Dimensionless blades volume for rotors with different number of blades – λ= 2.5.]*

3.2 BEM and CFD computations – Performance evaluation

Numerical simulations using BEM and CFD methods were carried out to evaluate the performance and the fluid flow patterns for typical rotors with 2, 3 and 4 blades (Figure 9).

The BEM simulations were obtained using QBLADE [32]. In that code, the BEMT equations are implemented in a robust and friendly simulation platform, equipped with a XFOIL interface for the polars curve computation. This numerical tool permits the performance analysis in the entire range of TSR, considering the corrections for tip and hub losses, as well as the Buhl-Glauert correction for high values of axial induction factor. All designed blades geometries were considered for the BEM simulations, using properly QBLADE setting parameters.

The CFD computations were performed ANSYS-CFX 15, with simulation domain shown in Figure (11). The k-ω/SST turbulence model was used in two different sub-domains: The first one is a parallelepiped that defines the large fluid region influenced by the turbine. The second one is an immersed cylindrical region that contains the runner. In this volume, the flow is described in a rotating reference frame with the same rotation speed of the turbine runner, in such a way the rotor rotation is taken into account by the action of Coriolis and Centrifugal accelerations. The simulations were performed always in a time-dependent flow regime.

The mesh generation was performed using the ANSYS-CFX/MESH software. Tetrahedral elements were used in an unstructured mesh, with local refinement in the wake and near wall regions, as illustrated by Figure (12). This refinement guarantees small values of the non-dimensional distance from the wall, y+, an important condition to assure good results for k-ω turbulence models. Table 1 presents three different mesh densities used for simulations of 4-blade rotors in the framework of a mesh convergence previous study. The convergence of Cp is achieved for meshes around 5.5 million nodes. The same mesh density was used for different runners, keeping the same refinement used for the reference condition (4-blade runner). The results obtained for the reference conditions realistically describe all the flow patterns (mainly the wake hydrodynamics) and had allowed good previsions of the machine performance, as also discussed in [33].

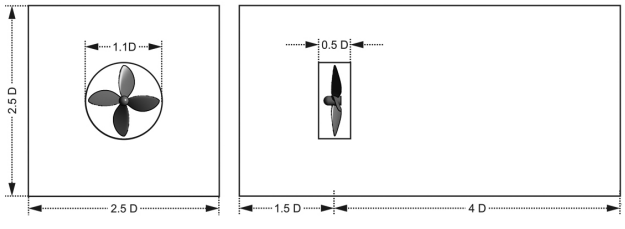

[Figure 11: CFD simulation –domain dimensions.]

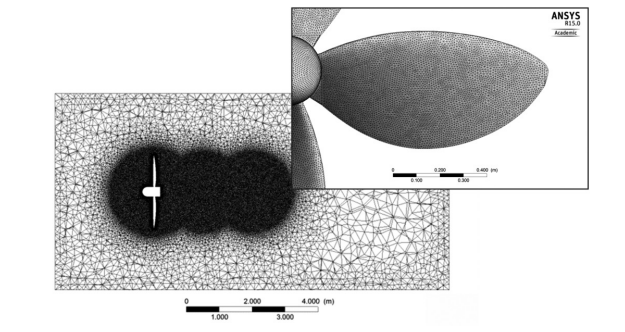

[Figure 12: CFD simulation – mesh details for 5.5 million nodes.]

[Table 1]: ***Different mesh sizes for 4-blade rotor with V_0=2.5 m/s and λ=1.6.***

	Mesh Nodes	y+	C_p
Mesh 1	426 216	323.6	0.381
Mesh 2	1 285 254	117.8	0.386
Mesh 3	5 572 162	1.6	0.389

In Table (2), numerical results for nominal conditions (V_0=2.5 m/s and λ=1.6) are summarized. The values of the power coefficient, obtained from CFD and BEM computations, are consistent with any number of blades.

Results for a wide range of TSR are presented in Figure (13). It could be observed that BEM and CFD simulations agree in the neighborhood of the nominal operation condition (λ=1.6). For higher values of TSR, the BEM results overestimate the performance of the turbine and it is more accentuated for the 2-blade rotor. For the 3-blade and 4-blade rotors, the performance levels are predicted coherently by the two approaches.

All results have shown an increase in the hydrodynamic performance for rotors with more blades, confirming some experimental considerations of a similar study of Dunquette et al [31] for wind turbines.

A slight difference in the power coefficient curve for 3-Blade or 4-Blade is observed. In a practical point of view, for hydrokinetic turbines, the small handicap of 3-blade rotor in comparison to the 4-blade rotor with less volume (Figure 11), induces the use of the last design choice considering the present value of nominal TSR.

[Table 2]: ***Performance of different rotors obtained by CFD and BEM with V_0=2.5 m/s and λ=1.6.***

	CFD	BEM
2-Blades	0.238	0.296
3-Blades	0.373	0.341
4-Blades	0.389	0.371

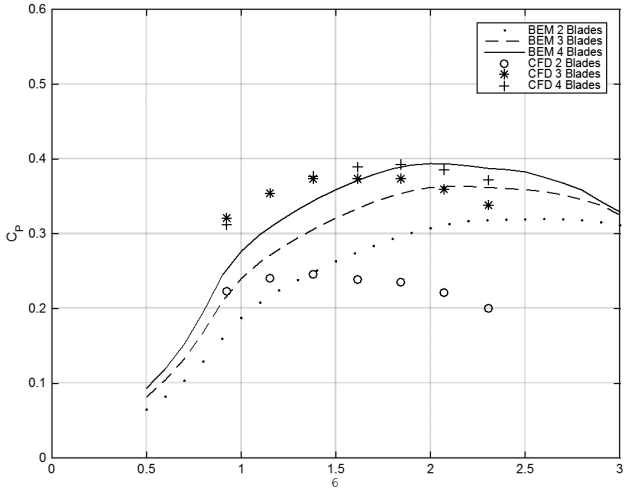

[Figure 13: CFD simulation –domain dimensions.]

3.3 Flow visualizations

In order to evaluate the hydrodynamic aspects of the fluid flow for differently designed runners, the flow patterns of the

wake flow are presented and discussed in this section. The flow visualizations are obtained from the post-processing of CFD computations. All flow visualizations are processed for the nominal condition for TSR.

In Figures (14), a general 3D flow visualization using streamlines and Q-criterion levels [34], illustrate the formation of the rotating wake for the different rotors. Tip and hub vortices can be identified. The tip vortex structure can also be observed in the 2D visualization of the axial velocity levels in the longitudinal plane (Figure (16)).

The extension of the wake influence region can be observed in Figure (17). The axial velocity levels and turbulence kinetic energy show that wake is larger for the rotors with more blades and the shadowing effects of the rotating blades are more pronounced in extension and in turbulence intensity.

Two-dimensional flow visualizations on circular cross sections are presented in Figures (18)-(19). A tomography of the levels of axial velocity and the kinetic energy of turbulence illustrate the influence of the wake in the rear region of the machines. The wake influence region is larger for 3 and 4-blade runners, but the levels of turbulence intensity are quite equivalent.

The tip vortices were properly identified. For 2-blade rotors, the transient variations in the wake are more intense. It can be verified in the thickness of vortices filaments shown in Figure (14).

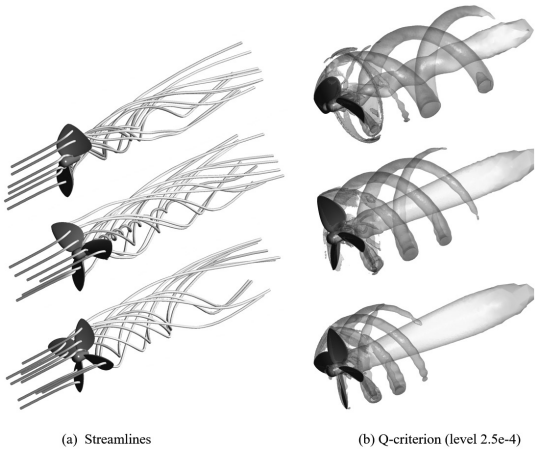

*[**Figure 14:** 3D flow visualizations.]*

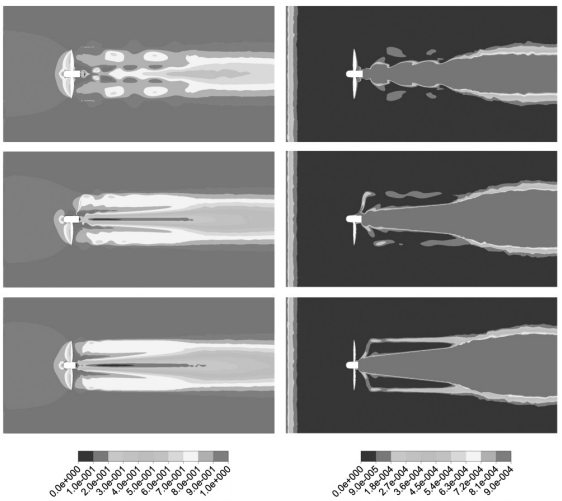

*[**Figure 15:** Visualization of dimensionless levels of axial velocity (u_x/U_0) and kinetic energy of turbulence (k/U_0^2.]*

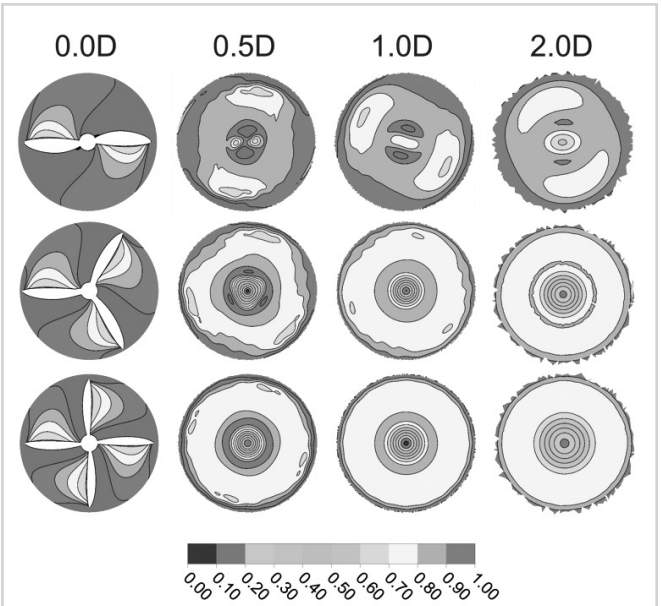

*[**Figure 16:** 2D cross sections visualizations of dimensionless axial velocity– u_x/V_0.]*

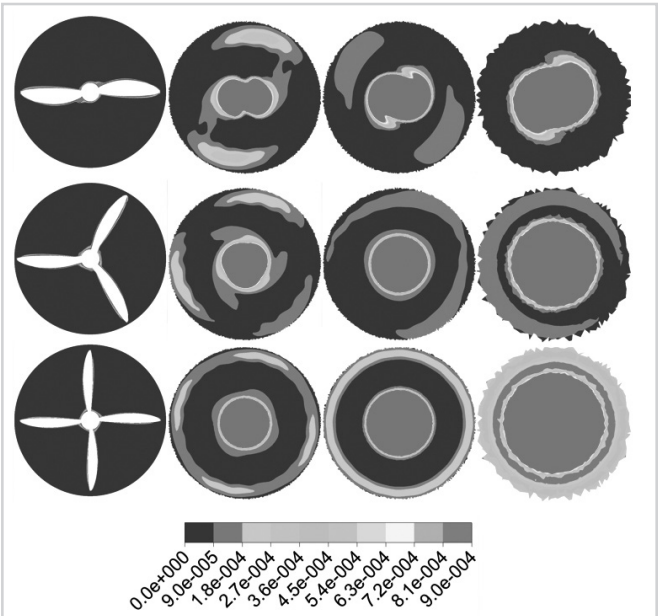

*[**Figure 17:** 2D cross sections visualizations of dimensionless kinetic energy of turbulence– k/V_0^2.]*

4. CONCLUSIONS

In this work the hydrodynamic influence of the number of blades in the propeller hydrokinetic turbines is discussed. The results have pointed out that better power coefficients are related to rotors with 3 or 4 blades. The classical Glauert-BEMT methodology produces thinner blades (with reduced volume) for runners with larger number of blades.

The difference in the performance of 3 and 4 blades runners is very small, indicating that from the hydrodynamic point of view these two runners are quite equivalent.

The flow visualization of the unsteady wake by means of the CFD results has shown the influence of the blade design in the wake region. Rotors with small number of blades trend to